Article

Controlled Supramolecular Assembly inside Living Cells by Sequential Multi-staged Chemical Reactions

Michaela Pieszka, Shen Han, Christiane Volkmann, Robert Graf, Ingo Lieberwirth, Katharina Landfester, David Y.W. Ng, and Tanja Weil

J. Am. Chem. Soc., **Just Accepted Manuscript** • DOI: 10.1021/jacs.0c05261 • Publication Date (Web): 19 Aug 2020

Controlled Supramolecular Assembly inside Living Cells by Sequential Multi-staged Chemical Reactions

Michaela Pieszka,[1,2] Shen Han,[1] Christiane Volkmann,[1] Robert Graf,[1] Ingo Lieberwirth,[1] Katharina Landfester,[1] David Y.W. Ng[1,*] and Tanja Weil.[1,2,*]

[1]Max Planck Institute for Polymer Research, Ackermannweg 10, 55128 Mainz, Germany

[2]Institute of Inorganic Chemistry I, Ulm University, Albert-Einstein-Allee 11, 89081 Ulm, Germany

Supramolecular Chemistry, Self-Assembly, Nanoscale Architectures, Boronic Acids, Peptides

ABSTRACT: Synthetic assembly within living cells represents an innovative way to explore purely chemical tools that can direct and control cellular behaviour. We use a simple and modular platform that is broadly accessible and yet incorporates highly intricate molecular recognition, immolative and rearrangement chemistry. Short bi-modular peptide sequences undergo a programmed sequence of events that can be tailored within the living intracellular environment. Each sequential stage of the pathways beginning with the cellular uptake, intracellular transport and localization imposes distinct structural changes that result in the assembly of fibrillar architectures inside cells. The observation of apoptosis, which is characterized by the binding of Annexin V, demonstrates that programmed cell death can be promoted by the peptide assembly. Higher complexity of the assemblies was also achieved by co-assembly of two different sequences, resulting in intrinsically fluorescent architectures. As such, we demonstrate that the in-situ construction of architectures within cells will broaden the community's perspective towards how structure formation can impact a living system.

INTRODUCTION

Supramolecular interactions govern core aspects of cellular life where they are omnipresent in every biological pathway. On the molecular level, non-covalent forces guide structure formation and biomolecular interactions, which can be seen within the DNA double helix, the secondary to quaternary structures of proteins, and the dipoles of lipids. Systematically, the individual assemblies propagate into interconnecting systems to perform DNA replication/transcription, protein folding/receptor interactions and shuttling molecules in and out of cells.[1] The resulting dynamics between these biological processes would thus define the fundamental elements of life (i.e. proliferation, homeostasis, metabolism).

As a whole, it is critical to realize that many of these assemblies elicit their function at the nanometer level, while their separate constituents are seemingly non-functional (i.e. nucleotides/DNA, fatty acids/vesicles, rRNA/ribosome).[1] Therefore, instead of using intrinsically bioactive components like proteins or DNA, the impact of nanoscience towards biology can also be realized through structure formation. Application wise, there has been a growing interest in methods to enrich and accumulate drug molecules within cells to circumvent efflux based drug resistance.[2, 3] As the rate of efflux of molecules is directly dependent on size,[4, 5] significant efforts have been made to direct drug/imaging molecules to form aggregates within cells[6, 7] and with promising in vivo results.[8, 9]

Nonetheless, the bioactivity of these systems often originates from known small molecule interactions such as from a chemotherapeutic agent or singlet oxygen production by metal complexes.[10, 11] In contrast, specific biological responses, like programmed cell death, driven purely by the formed self-assembled nanostructures are less known. We envisioned that the assembly of non-functional constituents into functional architectures directly in a living cell would not only be a significant milestone in nanobiotechnology, but also provide a platform to integrate synthetic chemistry with living processes.

Herein, we report the construction of two peptide sequences designed to undergo a multi-stage transformation that results in the assembly of fibrillar architectures inside cancer cells (Figure 1). The first stage, comprising the cellular entry process, is gated by a pH-dependent boronic acid-salicylhydroxamate complexation.[12] This chemistry links a transporter "TAT" sequence (trans-activator of transcription), derived from the human immunodeficiency virus (HIV),[13] together with a pro-assembling sequence (henceforth referred as depsipeptide). As such, upon successful endocytosis, the acidification within the intracellular vesicles releases the pro-assembling sequence. Here, the second and third stage is incorporated into the pro-assembling sequence, with the second stage guarded by an immolative boronic acid cage sensitive towards elevated or endogenous H_2O_2 within cancer cells.[14-16] Upon the immolation of the cage, the third stage is triggered by the *O,N*-acyl rearrangement of the depsipeptide that generates the linear isoleucine-serine-alanine (ISA) self-assembling motif.[17, 18] The production of ISA promotes the final stage of self-assembly into fibrillar architectures and in the process triggers apoptosis.

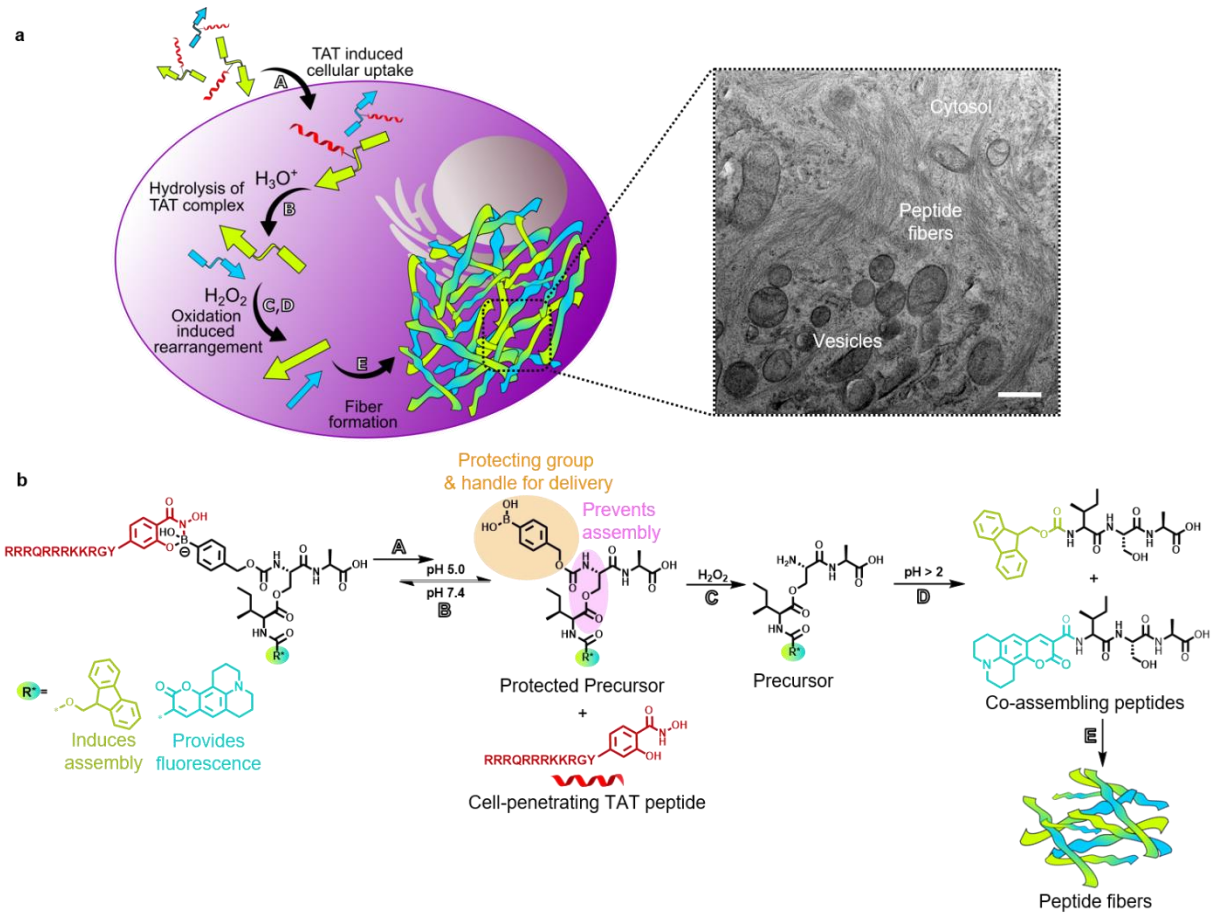

Figure 1: Intracellular co-assembly of peptides. a, Depsipeptides (kinked arrows) are uptaken by cells due to dynamic covalently bound salicylhydroxamate-TAT (SHA-TAT, red strang, step A). After hydrolysis of the complex in acidic environments (step B), the boronic acid head group of the depsipeptides is cleaved by intracellular hydrogen peroxide (step C). The subsequent *O,N*-acyl shift forms the linear co-assembling peptides (step D). The linear peptides (straight arrows) form fibrillar networks inside A549 cells (step E), which is visible by transmission electron microscopy (TEM, scale bar 500 nm). b, Chemical reactions that lead to cellular uptake, peptide linearisation and peptide co-assembly of Fmoc (green) and Coumarin 343 (blue) functionalised ISA.

In essence, the design comprises three modular components: (1) the pro-assembling depsi unit and its pH-reversible functionalisation with TAT, (2) the peroxide-triggered cleavage of the boronic acid masking group and the (3) pH-controlled *O,N*-acyl rearrangement to generate the self-assembling peptide sequence. In this way, intracellular transport, release and supramolecular assembly into peptide fibrils is individually and sequentially programmed inside different cellular compartments by consecutive chemical reactions (Figure 1).

Additionally, we demonstrate co-assembly as a strategy to increase the level of functionality by imparting fluorescence into the fibrillar structures to allow imaging.[19, 20] Co-assembly, i.e. the assembly of more than a single component, is prevalent in Nature and important examples include the assembly of α-/β-tubulin in microtubules[21], cholesterol/phospholipids in membranes[22] or the Arp2/3 complex in actins.[23] While Nature uses highly specific proteins to transport and program these assemblies, synthetic methods are advantageous as they can be bioorthogonal and also be specifically tailored. By incorporating sophisticated chemical designs into a simple bi-modular peptide sequence, we demonstrate that synthetic architectures can be formed directly within living systems using natural triggers.

RESULTS AND DISCUSSION

Solid phase peptide synthesis using fluorenylmethoxycarbonyl (Fmoc) chemistry was conducted with alanine preloaded Wang resin (Scheme 1). Fmoc-serine was added as the second amino acid using (benzotriazol-1-yloxy)tripyrrolidinophosphonium hexafluorophosphate (PyBOP) and N,N-diisopropylethylamine (DIPEA).[24] Importantly, Fmoc-serine was used without a protecting group on the hydroxyl group in order to create an ester bond with isoleucine later in the synthesis. After Fmoc deprotection of serine, the modification of the N-terminus using 4-(nitrophenyl)phenylboronic acid pinacol ester was performed. Fmoc-isoleucine was coupled on the amino acid side chain of serine using N,N′-diisopropylcarbodiimide (DIC) and 4-(dimethylamino)pyridine (DMAP), forming the ester and therefore the so called depsipeptide.[17] The peptide was removed from the solid support, and the boronic acid was deprotected simultaneously using a cleavage cocktail based on trifluoroacetic acid (TFA). After purification by

high-performance liquid chromatography (HPLC), the pure peptide **1a** was characterised by electrospray ionisation mass spectrometry (ESI-MS, Figure S6). In order to synthesise the fluorescent Depsi(C343-I)pba-SA (Depsi(Coumarin 343–isoleucine)phenylboronic acid–serine–alanine), the Fmoc group was removed using piperidine, and the peptide was modified with Coumarin 343 using PyBOP/DIPEA for activation before cleavage of the peptide from the solid support. The identity of the product **1b** was confirmed after HPLC purification by ESI-MS (Figure S9) which also showed that the peptide was isolated in high purity.

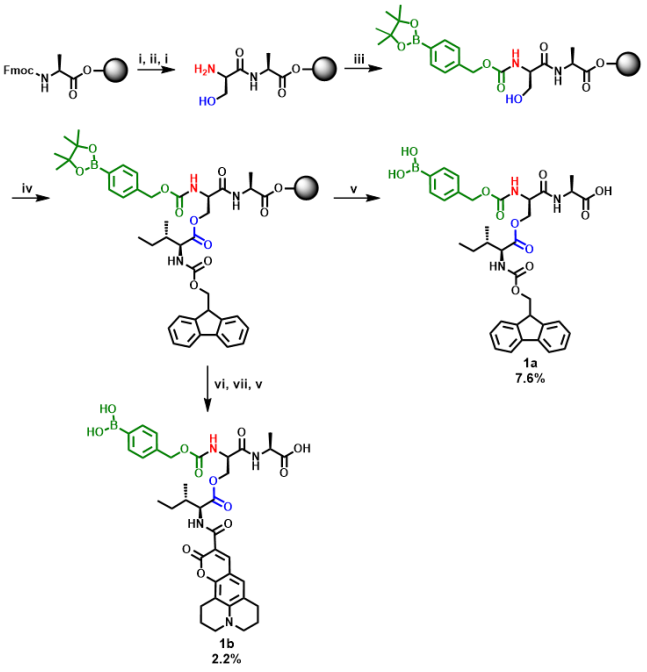

Scheme 1: Synthesis of depsipeptides Depsi(Fmoc-I)pba-SA **1a** and Depsi(C343-I)pba-SA **1b** by solid phase peptide synthesis. i) Piperidine, ii) Fmoc-Serine, PyBOP, DIPEA, iii) 4-(nitrophenyl)phenylboronic acid pinacol ester, iv) Fmoc-isoleucine, DIC, DMAP, v) TFA, triisopropylsilane, H_2O, vi) piperidine, vii) Coumarin 343, PyBOP, DIPEA.

In order to prove the hydrogen peroxide induced removal of the PBA protecting group and the subsequent *O,N*-acyl shift in solution outside cells, Depsi(Fmoc-I)pba-SA **1a** was incubated in NH_4HCO_3 buffer pH 7.4 with and without hydrogen peroxide (Figure *2* a-c, Figure S15). The peptide (R_T = 15.6 min) was stable in the absence of H_2O_2 and led to only 3% conversion into Fmoc-ISA **3a** (R_T = 14.6 min) within 45 h, due to slow hydrolysis of the carbamate bond. In contrast, addition of hydrogen peroxide led to a yield of 94% Fmoc-ISA **3a** in the same time. The intermediate Depsi(Fmoc-I)-SA **2a** could also be observed by the appearance of a peak at 14.0 min, which started to decrease after 8 h, while the product peak of **3a** increased. The same study was performed using Depsi(C343-I)pba-SA **1b** and the results showed that both – the removal of the phenylboronic acid by H_2O_2 as well as the *O, N*-acyl shift – were successful for the Coumarin derivative of the peptide (Figure 2 e, S16). After 4 h, Depsi(C343-I)pba-SA **1b** (R_T = 6.9 min) was no longer present, while the peaks for Depsi(C343-I)-SA **2b** (R_T = 5.0 min) and the linear peptide C343-ISA **3b** (R_T = 6.2 min) increased. After 24 h only **3b** was found in the sample. Incubation of Depsi(C343-I)pba-SA **1b** in NH_4HCO_3 buffer without H_2O_2 led to formation of only 3% of the linear peptide **3b**, which proves the stability of the peptide under these conditions (Figure 2 d).

TEM measurements of Depsi(Fmoc-I)pba-SA **1a** in phosphate buffer pH 7.4 after 24 h incubation with and without hydrogen peroxide showed the oxidation-triggered self-assembly of the peptide due to formation of the linear fibrillating sequence Fmoc-ISA **3a**, while the corresponding boronic acid modified depsipeptide **1a** did not form peptide fibers (Figure 2 f-g). In order to determine the critical fibrillation concentration of Fmoc-ISA **3a**, which is important for intracellular fiber formation, Fmoc-ISA was incubated at different concentrations ranging from 2 mM to 15 µM for 24 h in phosphate buffered saline (PBS). In TEM measurements, the lowest detectable concentration of peptide fibers was 62.5 µM (Figure S26).

The fluorescent peptide Depsi(C343-I)pba-SA **1b** was synthesized in order to enable live cell imaging of the peptide fibers, by co-assembly of both intracellularly rearranged peptides. While incubation of Depsi(C343-I)pba-SA **1b** in phosphate buffer did not lead to fiber formation, addition of H_2O_2 led to the appearance of amorphous aggregates in TEM (Figure 2 h-i). Co-incubation of both PBA depsipeptides upon hydrogen peroxide treatment at a ratio of 5:1 of **1a:1b** led to a mixture of fibres and some aggregates (Figure 2 j). Preliminary confirmation of co-assembly was accomplished by fluorescence microscopy, demonstrating the co-localization of the coumarin 343 signal with Proteostat, which detects cross-β-sheet containing peptide fibers (Figure 2 k). [19, 20, 24, 25]

Next, we elucidated the secondary structure of Fmoc-ISA as it is the primary driving force for fiber formation. To address this question, we performed Fourier-transform infrared spectroscopy measurements (Figure S29). The results indicated formation of β-sheets, due to the appearance of a maximum at 1634 cm^{-1}. Another maximum at 1688 cm^{-1} is usually assigned to antiparallel β-sheets in proteins but recently has been reported to derive from the carbamate bond of the Fmoc group. A shoulder which appeared at 1653 cm^{-1} in the FT-IR spectrum might be assigned to either α-helices or disordered structures.[26-29] ^{13}C (^1H) CP-MAS NMR spectra (cross polarisation-magic angle spinning nuclear magnetic resonance) confirmed the formation of three different competing structures by showing two sharp peaks and one broad peak for the Fmoc carbonyl, as well as several overlapping peaks for the C=O groups of the amino acids (Figure S30).

For additional proof of co-assembly of both peptides, circular dichroism spectroscopy, was used to visualize changes in the secondary structure (Figure 2 l). The CD spectrum of Fmoc-ISA **3a** in water showed a maximum at 218 nm, which can be attributed to a n->π*-transition and a shoulder peak at ~209 nm was observed in the CD spectrum, as well as a minimum at 190 nm.[30] Notably, a strong positive cotton effect was observed with a maximum at 267 nm, which corresponds to the π->π*-transition of the Fmoc groups in the self-assembled peptide fibers.[18] In contrast, the CD spectrum of C343-ISA **3b** revealed a maximum at 195 nm and a minimum at 215 nm, with opposite ellipticity compared to **3a**. In proteins these signals are attributed to β-sheets and correspond to π->π* and n->π*-transitions

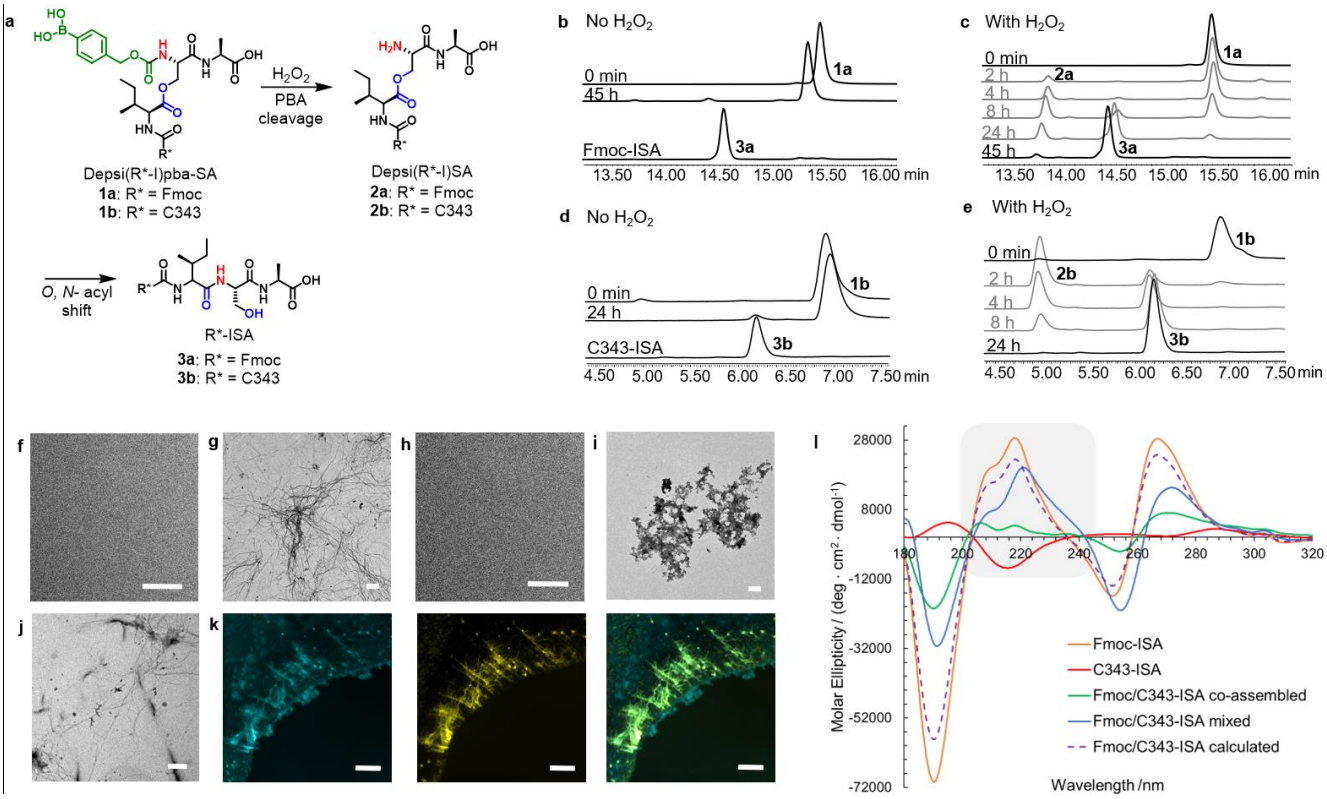

Figure 2: Hydrogen peroxide induced peptide fiber formation. a, Phenylboronic acid removal of Depsi(R*-I)pba-SA peptides **1a** and **1b** and subsequent *O,N*-acyl shift to give R*-ISA **3a** and **3b** (R*=Fmoc or Coumarin 343). b, HPLC spectra at different time points showing the stability of Depsi(Fmoc-I)pba-SA **1a** (15.6 min) in NH_4HCO_3 buffer and reference spectrum of Fmoc-ISA **3a** (14.6 min). c, H_2O_2 (2 mM) induced removal of the boronic acid to give Depsi(Fmoc-I)SA **2a** (14.0 min) and linearisation of the peptide to Fmoc-ISA **3a** (14.6 min). d, Stability of Depsi(C343-I)pba-SA **1b** (6.9 min) in buffer and HPLC spectrum of C343-ISA **3b** (6.2 min). e, H_2O_2 (1 mM) induced PBA removal and *O,N*-acyl shift of Depsi(C343-I)pba-SA **1b** (6.9 min) to first give Depsi(C343-I)SA **2b** (5.0 min) and finally C343-ISA **3b** (6.2 min). TEM images of: f, Depsi(Fmoc-I)pba-SA **1a**, g, Fmoc-ISA **3a**, h, Depsi(C343-I)pba-SA **1b,** i, C343-ISA **3b**, j, coincubation of Fmoc-ISA **3a** and C343-ISA **3b** 5:1. Scale bars 500 nm. k, Fluorescence microscope images of Fmoc-ISA:C343-ISA **3a**:**3b** 5:1. Left: Coumarin 343 channel (cyan), middle: Proteostat stained peptide fibers (yellow), right: merged Proteostat and Coumarin 343 channel showing the overlay of the fluorescent dyes (green). Scale bars 20 µm. l, Circular dichroism spectra of Fmoc-ISA (orange), C434-ISA (red) and their differently prepared assemblies in H_2O (co-assembled: green, mixed: blue.) Fmoc/C343-ISA (calculated, dashed purple line) is the sum of the separately recorded spectra of Fmoc-ISA and C343-ISA at a ratio of 5:1 to match the experimental conditions. The region of interest is highlighted in gray.

respectively.[31] For co-assembly, the study was accomplished using two different sample preparation methods – 1) the individual peptides (**3a** and **3b**) were first mixed before triggering the co-assembly in H_2O, and 2) the separate peptide assemblies are pre-formed in H_2O and the resultant nanostructures are combined. Mixing of the preformed nanostructures leads to appearance of an additional shoulder peak at ~235 nm and overall decrease in signal intensities. This effect is larger than expected from the spectral sum of a 5:1 mixture of **3a**:**3b**, which represents the hypothetical spectrum in absence of interactions between **3a** and **3b**. Hence, the results indicate interactions at the nanostructure level, causing a decrease in chirality of the assemblies. Upon coincubation of both peptides to induce co-assembly, the intensities of maxima and minima are further decreased significantly, which also includes signals attributed to electronic transitions of Fmoc groups. This is especially visible in the change of peak proportions at 218 and at 206 nm where the latter was previously observed as a shoulder at ~ 209 nm. We conclude that upon co-assembly of **3a** and **3b**, the overall structural chirality of the peptide assemblies is decreased leading to a comparable CD spectrum of **3a** due to the five-fold excess but with distinct differences in ellipticity.[32-34]

In order to provide cellular uptake of depsipeptides **1a/b** a salicylhydroxamate functionalized TAT peptide **12** was needed. TAT which has the amino acid sequence YGRKKRRQRRR, was synthesised by standard SPPS methods and was modified with 4-pentynoic acid on its N-terminus to first give molecule **11** (Figure S11). After a copper-catalysed azide–alkyne cycloaddition (CuAAC) with trityl (Trt) and (2-methoxyethoxy)methoxy (MEM) protected 4-azido salicylhydroxamate **10,** which was synthesised in seven synthetic steps (Figure S1), the peptide was cleaved from the solid support and purified by HPLC. After isolation of the pure peptide SHA-TAT **12**, it was characterised by MALDI-TOF mass spectrometry (matrix-assisted laser desorption/ionisation - time of flight, Figure S13).

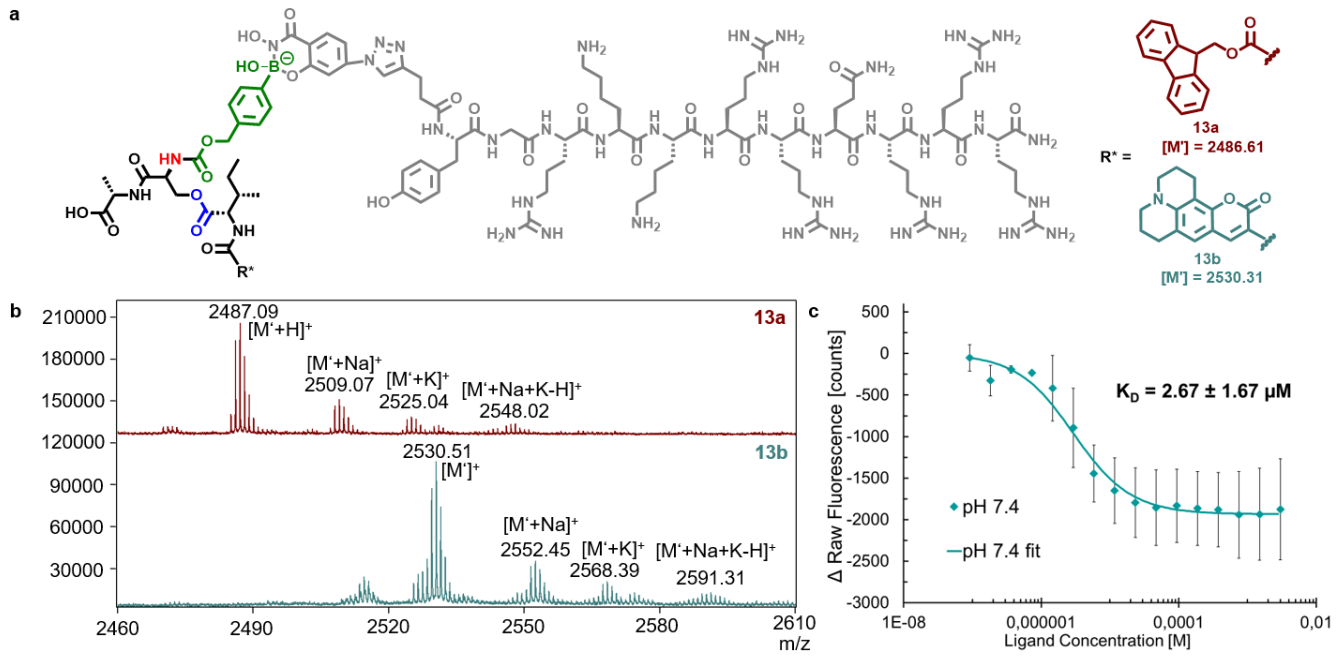

Figure 3: Complexes of SHA-TAT **12** and the boronic acid depsipeptides **1a** and **1b**. a, Chemical structure of dynamic covalently bound SHA-TAT and boronic acid modified depsipeptide conjugates **13a** and **13b**. b, MALDI spectra showing the successful formation of complexes of SHA-TAT **12** with Depsi(Fmoc-I)pba-SA **1a** (top) and Depsi(C343-I)pba-SA **1b** (bottom). [M'] corresponds to the molecular weight after loss of OH^-. [M']=[M–OH^-]. c, Determination of the K_D of the SHA-TAT complex with Depsi(C343-I)pba-SA (**13b**) by fluorescence quenching.

The attachment of the transporter peptide TAT was accomplished by boronic acid/salicyl hydroxamate chemistry. The formation of the dynamic covalent bond between the boronic acid functionalised depsipeptides **1a** and **1b** and SHA-TAT **12** in phosphate buffer pH 7.4 was proven by MALDI-TOF measurements for both Fmoc and C343 modified peptides **1a** and **1b**. Both products were formed by the condensation of PBA and SHA and multiple cation adducts were observed in the spectra (Figure 3 a-b). Fluorescence quenching experiments with Depsi(C343-I)pba-SA **1b** and SHA-TAT **12** gave an K_D of 2.67 µM, which was expected due to previously reported results for SHA-PBA complexes (Figure 3 c).[35] Reversibility of the complexation was accomplished at pH 5, which results in the recovery of fluorescence (Figure S31). The binding and release were confirmed by previous reports of our group to transport proteins into cells.[36, 37]

Alongside the acidification induced release of the pro-assembling sequence **1 a/b** from the TAT complexes **13 a/b** inside endosomes, the H_2O_2 stimulus is required for the assembly. The average concentration of H_2O_2 within A549 cells was assayed using the Intracellular Hydrogen Peroxide Assay Kit from Sigma-Aldrich and found to be 1.64 ± 0.16 µM (Figure S 57). Stimulation of H_2O_2 production can be performed with 100 nM of phorbol-12-myristat-13-acetate (PMA)[38] affording a 49% increase to 2.45 ± 0.37 µM. Using these conditions, the TAT-complexed depsipeptides **13 a/b** were incubated with A549 cells and the successful cellular uptake was shown by confocal microscopy (Figure 4 a). The concentration of the depsipeptides was adjusted to be 150 µM in total to meet the requirements of the critical fibrillation concentration. The depsipeptides were used at a ratio of 5:1 (**13a** : **13b)** in order to receive a sufficient fluorescence signal by Coumarin 343 inside cells, while maintaining an excess of the Fmoc peptides to direct the fiber formation. Incubation of cells with only the depsipeptides **1a** and **1b** did not show internalization of the peptides, which proves the necessity of SHA-TAT **12** for cellular uptake (Figure 4 a top row). The increase in fluorescence intensity of Coumarin 343 in the presence of PMA suggests local accumulation of fluorescent **3b** upon fiber formation indicating that the co-assembly was more pronounced at higher concentrations of H_2O_2, although as shown in Figure S47 and S48, peptide fiber formation also occurs without PMA. Significant cell deformation and nuclear condensation imply that cell viability is significantly affected (Figure S38, S39, S41). Incubation of the peptide samples with the cells for 2 h showed less cellular uptake, while extending it to 6 h led to more internalisation of the peptides (Figure S34). Peptide treated cells were also examined under higher magnification, where fibrillar structures inside the cell were visible in the Coumarin 343 channel (Figure S35). A striking observation was the inefficient staining of the nucleus in cells where the postulated assembly has occurred. This phenomenon has already been described in literature, where formation of peptide fibers inside cells prevented the staining of nuclei as nuclear stains were trapped inside fibrillar networks.[39]

We subsequently explored the mechanisms involved in each step of intracellular transport using time-lapsed Förster resonance energy transfer (FRET) and

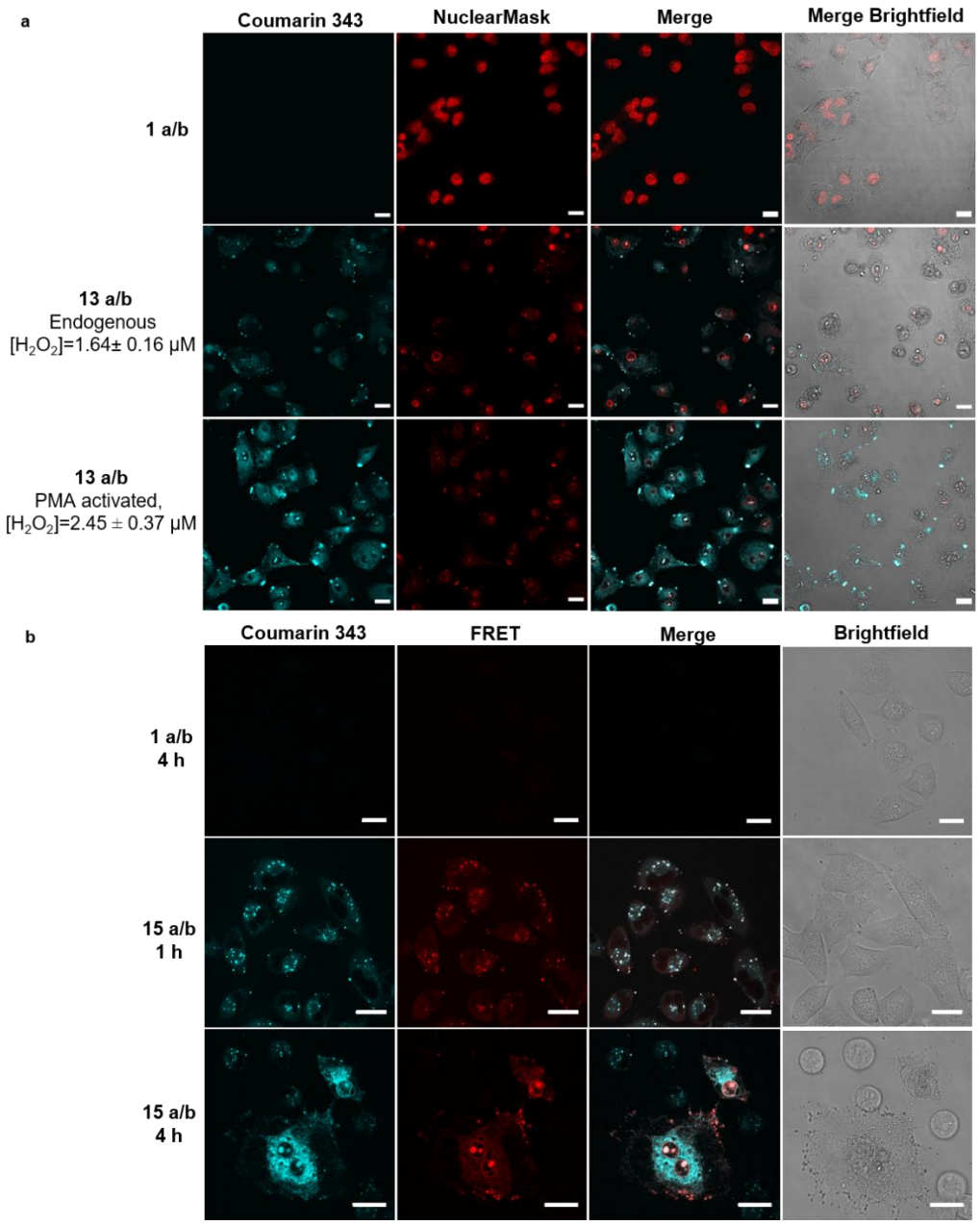

Figure 4: Cellular uptake and intracellular co-assembly of peptides. a, Confocal laser scanning micrographs of A549 cells treated for 4 h with only the depsipeptide mixture of **1a** and **1b** (top row) and treated with the addition of SHA-TAT **12** to induce cellular uptake without (middle row) and with PMA (bottom row). Scale bars 20 μm. b, Förster resonance energy transfer studies on A549 cells with **15 a/b** using Coumarin343 (donor, cyan) and 5-FAM (acceptor, red) as FRET pairs. Scale bars: 20 μm, λ_{ex} = 405 nm.

co-localization studies. TAT was labelled with 5-FAM (compound **14**) serving as the FRET acceptor for Coumarin 343 (Figure S14). Using this FRET labelled variant of **13 a/b,** named **15 a/b**, we performed confocal microscopy at 1 h and 4 h time points (Figure 4 c). At 1 h, uptake of **15 a/b** can be visualized as punctuated spots characteristic of vesicle based intracellular transport. A significant proportion of these vesicles exhibit FRET signals (red) suggesting that most of the uptaken **15 a/b** have not undergone dissociation. Nonetheless, a first indication of release into the cytosol was observed for a small proportion of these vesicles. At 4 h, among cells that are still intact, assembly has been accomplished in large areas of the cells. In these regions, FRET signals are absent, suggesting that **15 a/b** has been mostly dissociated into **1 a/b** and TAT **14** followed by the peroxide driven cascade. However, remaining amounts of undissociated **15 a/b** could be observed to proceed further along the TAT transportation pathway into the nuclear region. Here, the complex remains bound as the pH within the nucleus is no longer acidic.[40] The transport pathway through TAT-promoted endocytosis was confirmed using early/late endosome studies with CellLight™, which saw major co-localization (Figure S37).

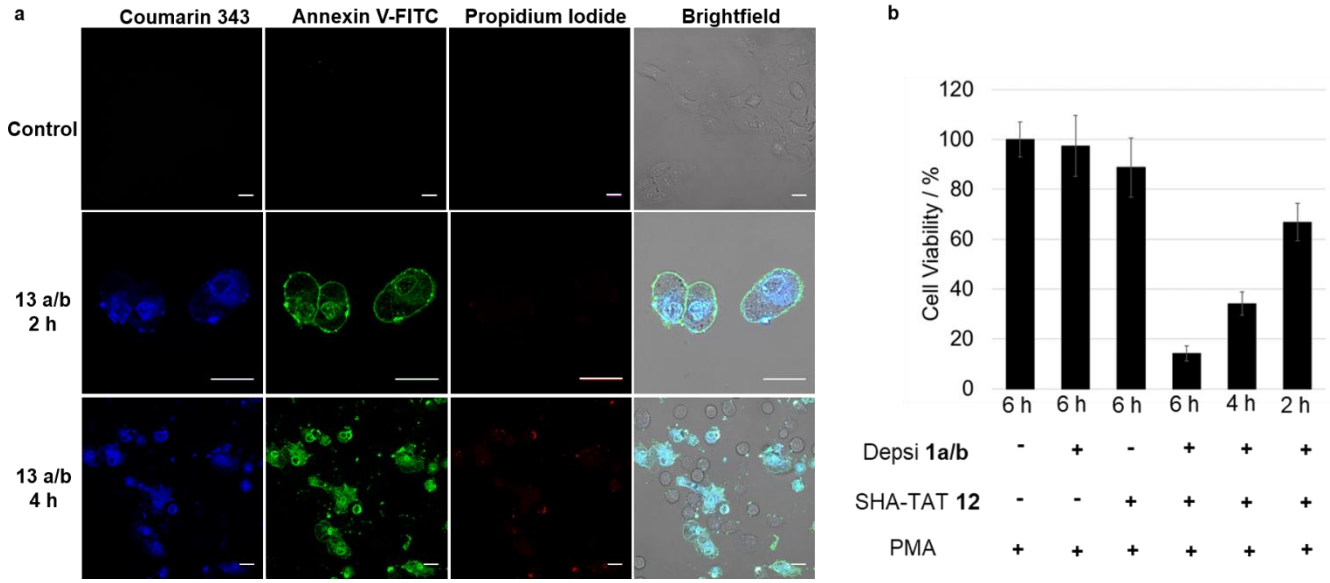

Figure 5: a, Apoptosis assay using Annexin V-FITC/propidium iodide on **13 a/b** and PMA treated A549 cells over 2 h and 4 h. Binding of Annexin V (green) towards the cell membrane was observed prominently at 2 h, demonstrating cells undergoing apoptosis due to the inversion of the phosphatidylserine motifs. Membrane collapse at 4 h was detected with the entry of propidium iodide (red) into the nucleus. Scale bars 20 µm. b, Cell viability of depsipeptides **1a** and **1b** and/or TAT **12** treated A549 cells determined by CellTiter-Glo Luminescent Cell Via-bility Assay. Cells were treated for different incubation times from 2-6 h with either only the depsipeptides **1a** and **1b**, only SHA-TAT **12** or both to create **13a** and **13b** at a concentration of 150 µM. A significant cytotoxic effect was observed for A549 cells treated with the depsipeptide-TAT complexes **13a** and **13b**. All samples were co-incubated with 100 nM PMA.

In addition, endosomal escape could also be visualized as diffused Coumarin 343 signals in the cytosol. Furthermore, nuclear transport of undissociated peptides **13 a/b**, demonstrated by SYTO™ RNASelect™ Green, was found to be localized inside the nucleolus, most likely due to the electrostatic attraction between TAT and DNA/RNA or perhaps hydrophobic interactions with the depsipeptides (Figure S40).[41] A previous report showed that self-assembling peptides might interact with RNA located inside the nucleoli.[42] In order to ascertain that the H_2O_2 driven assembly is specific towards the cytosol, we monitored the fiber formation using TEM at pH 5.0, 6.0 and 7.4 (Figure S23, S25). At both acidic pH values, corresponding to the early and late endosomes as well as lysosomes, H_2O_2 does not possess enough oxidative strength to initiate the reaction cascade for assembly. This pH dependent activity of H_2O_2 was reported in the literature.[43] As such, the acidic conditions within the endosomes specifically trigger the dissociation of **13 a/b**, while the cytosolic environment provides the condition for the oxidative cascade to initiate fiber formation. To demonstrate the molecular rearrangement of the depsipeptides inside cells, we analyzed cell lysates by HPLC and showed the H_2O_2 induced conversion of **1 b** to **3 b** (Figure S49).

The biological response of the cells to the intracellular assembly was subsequently investigated by Annexin-V/propidium iodide assay (Figure 5 a). Annexin-V is a protein that binds to phosphatidylserine, which is located on the external leaflet of the membrane structures exclusively during apoptosis.[44] The assay was conducted after 2 h and 4 h on A549 cells treated with **13 a/b**. At 2 h, Annexin-V was found to bind prominently to the cell membranes, indicating that affected cells are undergoing apoptosis. At this time frame, the integrity of the cell membrane still remains intact as propidium iodide failed to enter the cells. In contrast, at 4 h, propidium iodide signals were observed in the nuclear region due to its affinity to DNA.[44] This observation represented the membrane permeabilization process associated with late stage apoptosis. Analysis of cytotoxicity was accomplished using CellTiter-Glo Luminescent Cell viability assay, which is based on quantification of adenosine triphosphate (ATP) and therefore actively metabolising cells.[45] No significant toxic effects were observed after incubation of **1 a/b** at a concentration of 150 µM for 6 h with A549 cells (Figure 5 b). However, upon complexing with TAT to form **13 a/b**, significant impact towards cell viability was observed. Only 14% of cells were viable after 6 h, while incubation for 4 h or 2 h led to a viability of 34% and 66%, respectively. As the A549 cancer cells do produce intrinsic H_2O_2, transformation of **1 a/b** into **3a/b** still occurs in cells which are not treated with PMA and therefore the cell viability without PMA was 40% after 4 h (Figure S56), which is similar to the cell viability with addition of PMA. As the increase of hydrogen peroxide concentration by PMA stimulation (49%) does not cause a significant difference in cell viability, we conclude that non-stimulated cells already offer enough H_2O_2 to generate sufficient peptide fibers leading to effective apoptosis. Additionally, as known from β-amyloid structures, we believe that shorter fibers/protofibrils can already contribute to the apoptotic effects.[46]

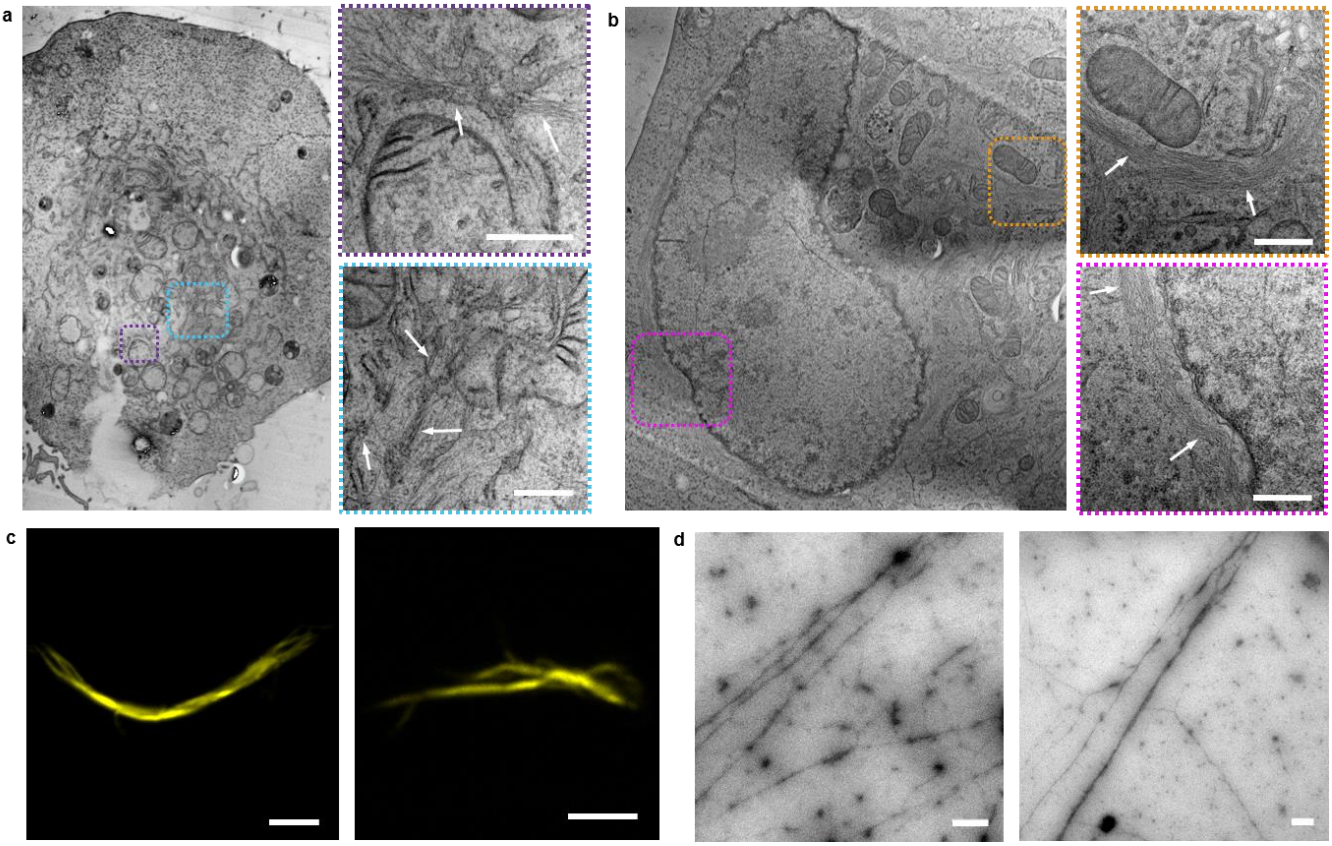

Figure 6: Intracellular peptide fiber formation. a, b, TEM micrographs of peptide fibers inside A549 cells (marked with dashed lines) after co-assembly of intracellularly generated Fmoc-ISA **3a** and C343-ISA **3b** and images of a cell, which were received after stitching TEM images together. Scale bars 500 nm. c, Fluorescence microscopy images of Proteostat stained peptide fibers after formation inside cells and extraction from the cells by lysis. Scale bars 5 µm. d, TEM micrographs of peptide fibers, which were received after lysis of depsipeptide TAT complex 1**3a** and **13b** treated A549 cells. Scale bars 500 nm.

Lastly, to visualize the intracellular fiber formation directly, **13 a/b** treated cells were fixed by high pressure freezing and subsequently freeze substitution was performed using acetone. After infiltration with epoxy resin and its polymerisation, sample blocks were sectioned into slices. The slices of the cells were examined in TEM (Figure 6 a and b). The formation of many dense peptide fiber networks was clearly visible inside the cells. Peptide fibrils were distributed inside the cell and were also observed to form next to the nucleus and mitochondria. To further show the formation of fibers, cells were lysed after treatment with the sample and the cell lysate was analysed by TEM and fluorescence microscopy (Figure 6 c and d).

Fibers were observed in TEM, which further proved the successful assembly of **3 a/b** inside cells. Furthermore, Proteostat staining of the cell lysate clearly showed formation of amyloid, cross-ß-sheet structures to which Proteostat is known to bind and coumarin343 fluorescent fibers could also be observed in the lysate (Figure S45, S46). Due to the resolution in the fluorescence microscope, only very thick fibers could be found in the cell lysate. Cell lysates of cells which were not treated with PMA but only with the complexes **13a/b** also contained fibers which shows that enhancing the intracellular H_2O_2 concentration with PMA is not necessary to induce peptide assembly, as cells naturally already produce hydrogen peroxide (Figure S47, S48).[33] TEM images of cells as well as cell lysate of A549 cells, which were not treated with the depsipeptide-TAT complexes **13a** and **13b**, did not show fibrillar structures, which demonstrates that fibers derived from the co-assembly of the intracellularly rearranged peptides Fmoc-ISA **3a** and C343-ISA **3b** (Figure S44, S54 and S55).

CONCLUSIONS

In summary, we have designed a peptide sequence that provides synthetic components for controlling cellular entry, intracellular dissociation and supramolecular assembly. The reactivity of each synthetic component within the peptide sequence is dictated by the intracellular localization where its immediate environment defines its chemistry and subsequent transport pathway. Consecutive reactions are initiated in a controlled fashion to afford co-assembling sequences that form fibrillar structures within the cytosol. The formation of these superstructures was imaged by fluorescence and electron microscopy and led to programmed cell death accompanied by nuclear fragmentation, actin disruption and membrane collapse. Furthermore, co-assembly features the potential of the nanosystem to dynamically customize functions and/or components to tune additional biological behavior. Collectively, the platform provides a broad accessibility and expands the domain of nanotechnology to directly impact living systems through structure formation.

ASSOCIATED CONTENT

Supporting Information. Materials and methods as well as extensive supplementary figures and data are available free of charge via the Internet at http://pubs.acs.org.

AUTHOR INFORMATION

Corresponding Author

* david.ng@mpip-mainz.mpg.de; weil@mpip-mainz.mpg.de

ACKNOWLEDGMENT

The project received funding from the Max Planck-Bristol Centre for Minimal Biology and the Volkswagen Foundation under project number 89943. The authors would like to thank Dr. Anke Kaltbeitzel for help with planning of the experiment and Christoph Sieber for sample preparation for TEM of cells, Dr. Gönül Kizilsavas for assigning NMR peaks, Jutta Schnee for measuring MALDI spectra and Jessica Wagner for measuring an APCI spectrum. We thank the reviewers for their efforts in stimulating additional experiments that improved the quality of the manuscript.

REFERENCES

1. Cragg, P. J., *Supramolecular Chemistry*. Springer Science+Business Media B.V. : Dordrecht, Heidelberg, London, New York, 2010.
2. Eckford, P. D. W.; Sharom, F. J., ABC Efflux Pump-Based Resistance to Chemotherapy Drugs. *Chem. Rev.* **2009,** *109* (7), 2989-3011.
3. Nikaido, H., Prevention of drug access to bacterial targets: permeability barriers and active efflux. *Science* **1994,** *264* (5157), 382.
4. Brownlee, W. J.; Seib, F. P., Impact of the hypoxic phenotype on the uptake and efflux of nanoparticles by human breast cancer cells. *Sci. Rep.* **2018,** *8* (1), 12318.
5. Shen, Z.; Wu, J.; Yu, Y.; Liu, S.; Jiang, W.; Nurmamat, H.; Wu, B., Comparison of cytotoxicity and membrane efflux pump inhibition in HepG2 cells induced by single-walled carbon nanotubes with different length and functional groups. *Sci. Rep.* **2019,** *9* (1), 7557.
6. Ng, D. Y. W.; Vill, R.; Wu, Y.; Koynov, K.; Tokura, Y.; Liu, W.; Sihler, S.; Kreyes, A.; Ritz, S.; Barth, H.; Ziener, U.; Weil, T., Directing intracellular supramolecular assembly with N-heteroaromatic quaterthiophene analogues. *Nat. Commun.* **2017,** *8* (1), 1850.
7. Qiao, S.-L.; Ma, Y.; Wang, Y.; Lin, Y.-X.; An, H.-W.; Li, L.-L.; Wang, H., General Approach of Stimuli-Induced Aggregation for Monitoring Tumor Therapy. *ACS Nano* **2017,** *11* (7), 7301-7311.
8. Nakamura, H.; Lee, A. A.; Afshar, A. S.; Watanabe, S.; Rho, E.; Razavi, S.; Suarez, A.; Lin, Y.-C.; Tanigawa, M.; Huang, B.; DeRose, R.; Bobb, D.; Hong, W.; Gabelli, S. B.; Goutsias, J.; Inoue, T., Intracellular production of hydrogels and synthetic RNA granules by multivalent molecular interactions. *Nat. Mater.* **2018,** *17* (1), 79-89.
9. Ye, D.; Shuhendler, A. J.; Cui, L.; Tong, L.; Tee, S. S.; Tikhomirov, G.; Felsher, D. W.; Rao, J., Bioorthogonal cyclization-mediated in situ self-assembly of small-molecule probes for imaging caspase activity in vivo. *Nat. Chem.* **2014,** *6* (6), 519-526.
10. Blunden, B. M.; Stenzel, M. H., Incorporating ruthenium into advanced drug delivery carriers – an innovative generation of chemotherapeutics. *J. Chem. Technol. Biotechnol.* **2015,** *90* (7), 1177-1195.
11. Cheng, Z.; Cheng, Y.; Chen, Q.; Li, M.; Wang, J.; Liu, H.; Li, M.; Ning, Y.; Yu, Z.; Wang, Y.; Wang, H., Self-assembly of pentapeptides into morphology-adaptable nanomedicines for enhanced combinatorial chemo-photodynamic therapy. *Nano Today* **2020,** *33*, 100878.
12. Shin, S. B. Y.; Almeida, R. D.; Gerona-Navarro, G.; Bracken, C.; Jaffrey, S. R., Assembling ligands in situ using bioorthogonal boronate ester synthesis. *Chem. Biol.* **2010,** *17* (11), 1171-1176.
13. Herce, H. D.; Garcia, A. E., Molecular dynamics simulations suggest a mechanism for translocation of the HIV-1 TAT peptide across lipid membranes. *Proc. Natl. Acad. Sci. USA* **2007,** *104* (52), 20805-20810.
14. Hagen, H.; Marzenell, P.; Jentzsch, E.; Wenz, F.; Veldwijk, M. R.; Mokhir, A., Aminoferrocene-based prodrugs activated by reactive oxygen species. *J. Med. Chem.* **2012,** *55* (2), 924-934.
15. Jourden, J. L. M.; Daniel, K. B.; Cohen, S. M., Investigation of self-immolative linkers in the design of hydrogen peroxide activated metalloprotein inhibitors. *Chem. Commun.* **2011,** *47* (28), 7968-7970.
16. Weinstain, R.; Savariar, E. N.; Felsen, C. N.; Tsien, R. Y., In Vivo Targeting of Hydrogen Peroxide by Activatable Cell-Penetrating Peptides. *J. Am. Chem. Soc.* **2014,** *136* (3), 874-877.
17. Coin, I.; Dölling, R.; Krause, E.; Bienert, M.; Beyermann, M.; Sferdean, C. D.; Carpino, L. A., Depsipeptide Methodology for Solid-Phase Peptide Synthesis: Circumventing Side Reactions and Development of an Automated Technique via Depsidipeptide Units. *J. Org. Chem.* **2006,** *71* (16), 6171-6177.
18. Tao, K.; Levin, A.; Adler-Abramovich, L.; Gazit, E., Fmoc-modified amino acids and short peptides: simple bio-inspired building blocks for the fabrication of functional materials. *Chem. Soc. Rev.* **2016,** *45* (14), 3935-3953.
19. Liu, X.; Cole, J. M.; Low, K. S., Molecular origins of dye aggregation and complex formation effects in coumarin 343. *J. Phys. Chem. C* **2013,** *117* (28), 14723-14730.
20. Rode, S.; Hayn, M.; Röcker, A.; Sieste, S.; Lamla, M.; Markx, D.; Meier, C.; Kirchhoff, F.; Walther, P.; Fändrich, M.; Weil, T.; Münch, J., Generation and characterization of virus-enhancing peptide nanofibrils

functionalized with fluorescent labels. *Bioconjugate Chem.* **2017,** *28* (4), 1260-1270.
21. Lewis, S. A.; Tian, G.; Cowan, N. J., The α- and β-tubulin folding pathways. *Trends Cell Biol.* **1997,** *7* (12), 479-484.
22. Ohvo-Rekilä, H.; Ramstedt, B.; Leppimäki, P.; Peter Slotte, J., Cholesterol interactions with phospholipids in membranes. *Prog. Lipid Res.* **2002,** *41* (1), 66-97.
23. Goley, E. D.; Welch, M. D., The ARP2/3 complex: an actin nucleator comes of age. *Nat. Rev. Mol. Cell Biol.* **2006,** *7* (10), 713-726.
24. Coste, J.; Le-Nguyen, D.; Castro, B., PyBOP®: A new peptide coupling reagent devoid of toxic by-product. *Tetrahedron Lett.* **1990,** *31* (2), 205-208.
25. Navarro, S.; Ventura, S., Fluorescent dye proteostat to detect and discriminate intracellular amyloid-like aggregates in escherichia coli. *Biotechnol. J.* **2014,** *9* (10), 1259-1266.
26. Fleming, S.; Frederix, P. W. J. M.; Ramos Sasselli, I.; Hunt, N. T.; Ulijn, R. V.; Tuttle, T., Assessing the Utility of Infrared Spectroscopy as a Structural Diagnostic Tool for β-Sheets in Self-Assembling Aromatic Peptide Amphiphiles. *Langmuir* **2013,** *29* (30), 9510-9515.
27. Jackson, M.; Mantsch, H. H., The use and misuse of FTIR spectroscopy in the determination of protein structure. *Crit. Rev. Biochem. Mol. Biol.* **1995,** *30* (2), 95-120.
28. Micsonai, A.; Wien, F.; Kernya, L.; Lee, Y.-H.; Goto, Y.; Réfrégiers, M.; Kardos, J., Accurate secondary structure prediction and fold recognition for circular dichroism spectroscopy. *Proc. Natl. Acad. Sci. USA* **2015,** *112* (24), E3095-E3103.
29. Wei, G.; Su, Z.; Reynolds, N. P.; Arosio, P.; Hamley, I. W.; Gazit, E.; Mezzenga, R., Self-assembling peptide and protein amyloids: from structure to tailored function in nanotechnology. *Chem. Soc. Rev.* **2017,** *46* (15), 4661-4708.
30. Argudo, P. G.; Contreras-Montoya, R.; Álvarez de Cienfuegos, L.; Cuerva, J. M.; Cano, M.; Alba-Molina, D.; Martín-Romero, M. T.; Camacho, L.; Giner-Casares, J. J., Unravelling the 2D self-assembly of Fmoc-dipeptides at fluid interfaces. *Soft Matter* **2018,** *14* (46), 9343-9350.
31. Jiang, J.; Abramavicius, D.; Bulheller, B. M.; Hirst, J. D.; Mukamel, S., Ultraviolet spectroscopy of protein backbone transitions in aqueous solution: combined QM and MM simulations. *J. Phys. Chem. B* **2010,** *114* (24), 8270-8277.
32. Horgan, C. C.; Rodriguez, A. L.; Li, R.; Bruggeman, K. F.; Stupka, N.; Raynes, J. K.; Day, L.; White, J. W.; Williams, R. J.; Nisbet, D. R., Characterisation of minimalist co-assembled fluorenylmethyloxycarbonyl self-assembling peptide systems for presentation of multiple bioactive peptides. *Acta Biomater.* **2016,** *38*, 11-22.
33. Mu, X.; Eckes, K. M.; Nguyen, M. M.; Suggs, L. J.; Ren, P., Experimental and Computational Studies Reveal an Alternative Supramolecular Structure for Fmoc-Dipeptide Self-Assembly. *Biomacromolecules* **2012,** *13* (11), 3562-3571.
34. Smith, D. K., Lost in translation? Chirality effects in the self-assembly of nanostructured gel-phase materials. *Chem. Soc. Rev.* **2009,** *38* (3), 684-694.
35. Zegota, M. M.; Wang, T.; Seidler, C.; Ng, D. Y. W.; Kuan, S. L.; Weil, T., "Tag and Modify" protein conjugation with dynamic covalent chemistry. *Bioconjugate Chem.* **2018,** *29* (8), 2665-2670.
36. Seidler, C.; Ng, D. Y. W.; Wu, Y.; Weil, T., pH responsive supramolecular core-shell protein hybrids. *Supramol. Chem.* **2016,** *28* (9-10), 742-746.
37. Seidler, C.; Zegota, M. M.; Raabe, M.; Kuan, S. L.; Ng, D. Y. W.; Weil, T., Dynamic core–shell bioconjugates for targeted protein delivery and release. *Chem. Asian J.* **2018,** *13* (22), 3474-3479.
38. Kuwabara, W. M. T.; Zhang, L.; Schuiki, I.; Curi, R.; Volchuk, A.; Alba-Loureiro, T. C., NADPH oxidase-dependent production of reactive oxygen species induces endoplasmatic reticulum stress in neutrophil-like HL60 cells. *PLOS ONE* **2015,** *10* (2), e0116410.
39. Zhou, J.; Du, X.; Yamagata, N.; Xu, B., Enzyme-instructed self-assembly of small D-peptides as a multiple-step process for selectively killing cancer cells. *J. Am. Chem. Soc.* **2016,** *138* (11), 3813-3823.
40. Llopis, J.; McCaffery, J. M.; Miyawaki, A.; Farquhar, M. G.; Tsien, R. Y., Measurement of cytosolic, mitochondrial, and Golgi pH in single living cells with green fluorescent proteins. *Proc. Natl. Acad. Sci. USA* **1998,** *95* (12), 6803-6808.
41. Audas, Timothy E.; Jacob, Mathieu D.; Lee, S., Immobilization of Proteins in the Nucleolus by Ribosomal Intergenic Spacer Noncoding RNA. *Molecular Cell* **2012,** *45* (2), 147-157.
42. Wang, H.; Feng, Z.; Tan, W.; Xu, B., Assemblies of D-peptides for targeting cell nucleolus. *Bioconjugate Chem.* **2019,** *30* (10), 2528-2532.
43. Bruice, T. C.; Zipplies, M. F.; Lee, W. A., The pH dependence of the mechanism of reaction of hydrogen peroxide with a nonaggregating, non-mu-oxo dimer-forming iron (III) porphyrin in water. *Proc. Natl. Acad. Sci. USA* **1986,** *83* (13), 4646.
44. Demchenko, A. P., Beyond annexin V: fluorescence response of cellular membranes to apoptosis. *Cytotechnology* **2013,** *65* (2), 157-172.
45. Hannah, R.; Beck, M.; Moravec, R.; Riss, T., CellTiter-Glo™ luminescent cell viability assay: A sensitive and rapid method for determining cell viability. *Promega Cell Notes* **2001,** *2*, 11-13.
46. Jan, A.; Adolfsson, O.; Allaman, I.; Buccarello, A.-L.; Magistretti, P. J.; Pfeifer, A.; Muhs, A.; Lashuel, H. A., Aβ42 Neurotoxicity Is Mediated by Ongoing Nucleated Polymerization Process Rather than by Discrete Aβ42 Species. *J. Biol. Chem.* **2011,** *286* (10), 8585-8596.

Insert Table of Contents artwork here